Hassan Falah Hassan[*], *Mohammed Husein Al-Dahlaki, Ali Alsajad Ibrahim*

SHEAR BEHAVIOUR OF FIBROUS NORMAL AND HIGH STRENGTH CONCRETE BEAMS REINFORCED BY GFRP BARS AND STIRRUPS

OSOBINE SMICANJA KOD VLAKNASTIH NORMALNIH BETONSKIH NOSAČA POVIŠENE ČVRSTOĆE OJAČANIH GFRP ARMATUROM I UZENGIJAMA

Originalni naučni rad / Original scientific paper
UDK /UDC:

Rad primljen / Paper received: 28.09.2021

Adresa autora / Author's address:
Al-Mustansiriyah University, Faculty of Engineering, Civil Engineering Department, Baghdad, Iraq
[*]email: hassanfala@gmail.com

Keywords
- shear stress
- high strength concrete beams
- GFRP bars and stirrups
- cracks
- CSA and ISIS codes and practice

Ključne reči
- napon smicanja
- betonske grede povišene čvrstoće
- GFRP armatura i uzengije
- prsline
- CSA i ISIS standardi i primena

Abstract

The glass fibre reinforced polymers (GFRP) can be used to produce reinforcement bars used as suitable alternatives for conventional steel reinforcement due to its reasonable strength/weight ratio and corrosion resistance. The fibre reinforced concrete (FRC) is a kind of concrete that can be fabricated by adding steel fibre to the concrete mix to enhance the mechanical potential and consequent structural performance. This study is presented to inspect shear performance of fibrous concrete beams reinforced by GFRP bars and stirrups. Such a programme includes casting and testing 16 reinforced concrete beams. GFRP stirrups reinforce 15 beams; however, one beam is reinforced by the steel stirrup as a reference beam. The variables of this study comprise the content of steel fibres, shear reinforcement ratio, and concrete compressive strength; the beams are divided into five groups according to test parameters. Experimental results show that increasing the shear reinforcement ratio from 0.222 to 0.443 % increases the failure load by 8, 10, and 11 % for steel fibre content 0, 0.5, and 1 %, in respect. Also, results show that increasing compressive strength of concrete from 30 to 70 MPa increases failure load by 28, 40, and 42 % for steel fibre content 0, 0.5, and 1 %, in respect. Increasing steel fibres content from 0 to 1 % increases the failure load by 8 to 18.9 %. It is found that increase of compressive strength of concrete from 30 to 70 MPa decreases strain in GFRP stirrups between 60-125 %, while increase in shear reinforcement ratio from 0.222 to 0.443 decreases the strain in GFRP stirrups and bars between 5-64 %. Furthermore, the crack width decreases by 32-108 % when steel fibre content is raised from 0 to 1 % for all tested beams. The experimental and calculated ultimate shear load comparison shows that CSA S806-12 and ISIS-07 codes results are very conservative, with a safety factor reaching 66 %. In contrast, the ACI440-1R-15 and Tureyen equation code results show good agreement with experimental results.

Izvod

Polimeri ojačani staklenim vlaknima (GFRP) se mogu upotrebiti za izradu armature za ojačanje kao zadovoljavajuću alternativa konvencionalnim čeličnim armaturama zbog prihvatljivog odnosa čvrstoća/težina i korozione otpornosti. Vlaknasto ojačani beton (FRC) je tip betona koji se može izraditi dodavanjem čeličnih vlakana u betonsku mešavinu radi poboljšanja mehaničkih osobina i odgovarajućih osobina konstrukcije. U radu je predstavljeno ispitivanje osobina smicanja vlaknastih betonskih nosača ojačanih GFRP armaturom i uzengijama. Program ispitivanja obuhvata izlivanje i ispitivanje 16 ojačanih betonskih greda. GFRP uzengijama je ojačano 15 greda; međutim, jedan nosač je ojačan čeličnom uzengijom kao referentni nosač. U radu su promenljive veličine: sastav čeličnih vlakana, odnos smicajnog ojačanja i pritisna čvrstoća betona; nosači su podeljeni u pet grupa prema parametrima ispitivanja. Eksperimentalni rezultati pokazuju da sa porastom odnosa ojačanja smicanja od 0,222 do 0,443 % raste opterećenje loma za 8, 10, i 11 % za sastav čeličnog vlakna od 0, 0,5 i 1 %, respektivno. Takođe, rezultati pokazuju da porast pritisne čvrstoće betona od 30 do 70 MPa povećava opterećenje loma za 28, 40 i 42 % za sastav čeličnih vlakana 0, 0,5 i 1 %, respektivno. Povećanje sastava čeličnih vlakana od 0 do 1 % povećava opterećenje pri lomu za 8 do 18,9 %. Porast pritisne čvrstoće betona od 30 do 70 MPa smanjuje deformacije u GFRP uzengijama za 60-125 %, dok se sa porastom odnosa smicajnog ojačanja sa 0,222 na 0,443, smanjuju deformacije u GFRP uzengijama i armaturi za 5-64 %. Osim toga, širina prsline se smanjuje za 32-108 % kada se poveća sadržaj čeličnih vlakana sa 0 na 1 % za sve ispitane grede. Poređenjem podataka smicajne čvrstoće dobijenih eksperimentalno i računski pokazuje da su vrlo konzervativni rezultati dobijeni standardima CSA S806-12 i ISIS-07, sa stepenom sigurnosti koji dostiže 66 %. S druge strane, proračuni prema ACI440-1R-15 i Turejen izrazom daju rezultate koji se dobro slažu sa eksperimentalnim rezultatima.

INTRODUCTION

Deterioration of concrete structures due to the corrosion of steel reinforcement has led to the need for an alternative type of reinforcement such as fibre-reinforced-polymer (FRP) reinforcement. Stirrups used for shear reinforcement usually are located as outer reinforcement with respect to the flexural reinforcement. Therefore, they are more susceptible to severe environmental effects because of the minimum concrete cove provided /1-4/. FRPs are corrosion-free materials and have recently been used as reinforcement to avoid the deterioration of concrete structures caused by corrosion of steel reinforcement. The use of FRP as reinforcement for concrete structures has increased rapidly over the last ten years. FRP reinforcement is made from high-tensile-strength fibres such as carbon, glass, aramid, and others embedded in polymeric matrices and produced in the form of bars, strands, ropes, tendons, and grids in a wide variety of shapes and characteristics /5-7/. FRP reinforcement is used as prestressed, non-prestressed, and shear reinforcement for concrete structures. Several experimental and analytical research programs have been conducted to investigate the flexural behaviour of concrete members reinforced and/or prestressed by FRP reinforcement. The use of FRP as shear reinforcement for concrete structures has not yet been fully explored, and currently available data are not sufficient to formulate rational design guidelines, /8-12/.

Since FRP reinforcement is characterised by a linearly elastic stress-strain relationship up to failure, shear failure of reinforced concrete members will occur due either rupture of FRP stirrups or crushing of concrete in the compression zone or the web. Failure due to rupture of FRP stirrups will occur suddenly when one or more FRP stirrups reach their strength capacity. This type of shear failure is brittle when compared to that of a beam reinforced with steel stirrups. The other mode of failure, shear-compression failure, occurs when diagonal shear cracks propagate towards the compression chord, reducing the depth of the compression zone and causing crushing of the concrete. Such a mode of failure is much more comparable to that of a concrete beam with steel stirrups. Concrete members reinforced with steel stirrups are typically designed for shear to yield the steel stirrups before concrete crushing. Due to the diagonal nature of shear cracks, the induced tensile forces are typically oriented at an angle regarding the stirrups to prevent tensile strength development. The bending of FRP stirrups to develop sufficient anchorage may also lead to a significant reduction in the strength capacity of the stirrups, /13-17/.

Kotynia et. al. /18/ experimentally tested twelve T-shaped concrete beams reinforced with glass fibre reinforced polymer (GFRP) or steel bars without stirrups. The aim of this research is to analyse the influence of a type of longitudinal reinforcement (GFRP or steel) on shear capacity and deformability of concrete beams without stirrups and to investigate a dowel effect of the reinforcement on the shear strength. Results show that the steel reinforced beams reached much higher ultimate shear strength than GFRP reinforced beams, both GFRP and steel RC beams were not susceptible to changes of reinforcement ratio if the reinforcement ratio was below 1.40 %. Application of the GFRP longitudinal tensile reinforcement in two layers delayed the shear failure and increased the shear strength by near 28 %, beams reinforced with GFRP indicated higher ductility than beams reinforced with steel. Jumaa, et. al. /19/ tested six large-scale high-strength concrete beams reinforced with basalt fibre reinforced polymer (BFRP) bars and stirrups and three corresponding beams without stirrups were constructed and tested for shear failure under four-point bending. The main parameters considered were the beam effective depth (300, 500, and 700 mm) and stirrup spacing. Result show that the presence of BFRP stirrups reduces the crack spacing to 0.36 *d*, compared to 0.52 *d* in beams without stirrups. Reducing the stirrup spacing from *d*/2 to *d*/3 resulted in a decrease in shear crack width, particularly in small and medium beams. The presence of BFRP stirrups does not suppress the size effect completely, as the initial shear crack, shear crack width, shear resistant components analysis, strain in the BFRP stirrups, and normalised shear strength are still affected by beam depth. Li, et. al. /20/ studied the shear behaviour of 15 concrete beams reinforced in shear with CFRP-MF (mesh fabric) configuration or with/without steel stirrups (as control specimens). The section dimensions of the specimens were 300 mm height × 150 mm width. The length of concrete beams varied as per the shear span-to-effective depth ratio. The shear span-depth ratios were 1.0, 2.5, and 3.5 and the beam lengths were 1800, 1800 and 2200 mm, respectively. The failure mode of concrete beams reinforced with CFRP-MF still depended on shear span/depth ratio of concrete beams. CFRP-MF ruptured either near the flexural reinforcement or crossing by the dominate diagonal cracks. CFRP-MF stirrups turned out to be more effective at confining core concrete than steel stirrups, thereby obtaining a larger efficiency factor in deep beams.

TEST SPECIMENS

Sixteen beams are cast and tested in this research. Each simply supporting concrete beam has a rectangular section of 150×200 mm with total length of 1550 mm. The beams are simply supported over one span of 1450 mm centre to centre between two supports, and a 50 mm overhang. Figure 1 shows details of the tested beam. The studied parameters in the test are: shear reinforcement ratio ρ_{vf}; concrete compressive strength; steel fibre content V_f.

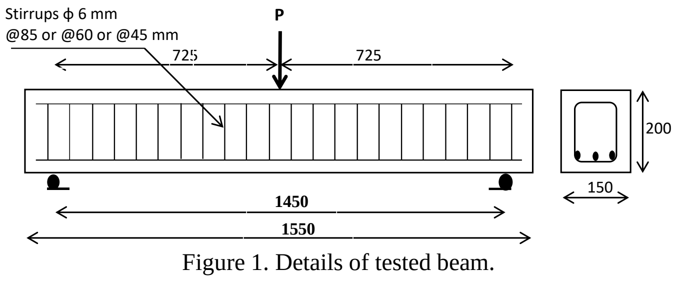

Figure 1. Details of tested beam.

Beam designations are as follows: B for beam; R reference; 30, 50, and 70 for compressive strength of concrete; 0.5*d*, 0.33*d*, and 0.25*d* for spacing in stirrups; 0 %, 0.5 % and 1 % for steel fibre content. For example, the following code B30-0.5d-0 indicates that the beam has a concrete compressive strength of 30 MPa, spacing of stirrup 0.5*d*, 0 % steel fibre content. Table 1 shows the tested beams' details.

Table1 Characteristics of the tested beams

Beam specimen	Beam dimensions		Total beam length (mm)	Target concrete strength (MPa)	Steel fibre %	Bottom reinforcements (GFRP bars) (mm)	Stirrups spacing (mm)
	B (mm)	h (mm)					
BR30-0.5d-0 (Reference)	150	200	1550	30	0	3φ16	6@85[a]
B30-0.5d-0 B30-0.5d-0.5 B30-0.5d-1				30	0 0.5 1	3φ16	6@85
B30-0.33d-0 B30-0.33d-0.5 B30-0.33d-1				30	0 0.5 1	3φ16	6@60
B30-0.25d-0 B30-0.25d-0.5 B30-0.25d-1				30	0 0.5 1	3φ16	6@40
B50-0.5d-0 B50-0.5d-0.5 B50-0.5d-1				50	0 0.5 1	3φ16	6@85
B70-0.5d-0 B70-0.5d-0.5 B70-0.5d-1				70	0 0.5 1	3φ16	6@85

[a] Reference beam with steel stirrups.

MIX PROPORTIONS

Concrete mixtures are obtained by preparing locally available raw materials such as cement, sand, gravel, water, etc. The materials are mixed using an electric mixer of 0.20 m^3 capacity.

The concrete production of targeted compressive strengths is of 30, 50, and 70 MPa. Mixing ratios of raw materials for each mix are illustrated in Table 2. Mixtures are designed according to the ACI-211.1-91, /21/.

Table 2. Mixture design characteristics.

Target concrete strength (MPa)	Cement kg/m^3	Gravels kg/m^3	Silica fumes kg/m^3	W/C	Sand kg/m^3	Viscocrete PC 20 kg/m^3
30	400	1200	---	0.45	550	---
50	575	767	45	0.3	880	22.5
70	650	500	90	0.22	900	26

ULTIMATE LOAD CAPACITY

Ultimate load capacities, first crack load, the midspan deflection, and failure type of all the tested beams are given in Table 3.

Effects of shear reinforcement upon ultimate load

Table 4 and Fig. 2 show when f'c = 30 MPa and the steel fibre ratio 0 %, the failure load increases by 0, 7, 8 % when ρ_{vf} % increases from 0.222 to 0.333, and 0.443, respectively, and when the steel fibre ratio 0.5 %, the failure load increases by 0, 6, 9 % when ρ_{vf} % increases from 0.222 to 0.333, and 0.443, respectively. While when the steel fibre ratio 1 %, the failure load increases by 0, 5, 11 % when ρ_{vf} % increases from 0.222 to 0.333, and 0.443, respectively.

Table 3. Experimental results and modes of failure.

Beam specimen	ρ_{vf} %	f'c (MPa)	Initial crack loading, P_{cr} (kN)	failure load, Pu (kN)	P_{cr}/Pu	Mid-span deflection at failure (mm)	modes of failure [a]
BR30-0.5d-0 (Reference)	0.222	30	21.5	76.5	0.28	11.98	C.C+S.F
B30-0.5d-0 B30-0.5d-0.5 B30-0.5d-1	0.222	30	20 22 23.5	76 82.5 87.5	0.26 0.27 0.268	12.5 13.4 11.8	C.C+S.F FF +S.F FF +S.F
B30-0.33d-0 B30-0.33d-0.5 B30-0.33d-1	0.333	30	18.5 20 22.5	81 87.5 92.5	0.23 0.22 0.24	11.8 11.5 11.9	C.C+S.F FF+S.F FF+S.F
B30-0.25d-0 B30-0.25d-0.5 B30-0.25d-1	0.443	30	17.5 21.5 24	82 90.5 97.5	0.21 0.23 0.25	11.95 12.85 11.2	FF+S.F FF +S.F FF+S.F
B50-0.5d-0 B50-0.5d-0.5 zB50-0.5d-1	0.222	50	24 25 27	88 108.5 119.5	0.27 0.23 0.22	10.8 9.98 10.25	S.F FF+S.F FF+S.F
B70-0.5d-0 B70-0.5d-0.5 B70-0.5d-1	0.222	70	24 26 27.5	97 115.5 124.5	0.25 0.23 0.22	11.1 11.4 10.6	S.F S.F FF+S.F

[a] C.C = crushing of concrete; S.F = shear failure; FF = flexural failure

Table 4. Effects of shear reinforcement on the failure load.

Beams	f'c (MPa)	V_f %	ρ_{vf} %	Failure load, Pu (kN)	Increase of Pu (%)
B30-0.5d-0	30	0	0.222	76	0
B30-0.33d-0			0.333	81	7
B30-0.25d-0			0.443	82	8
B30-0.5d-0.5	30	0.5	0.222	82.5	0
B30-0.33d-0.5			0.333	87.5	6
B30-0.25d-0.5			0.443	90.5	9
B30-0.5d-1	30	1	0.222	87.5	0
B30-0.33d-1			0.333	92.5	5
B30-0.25d-1			0.443	97.5	11

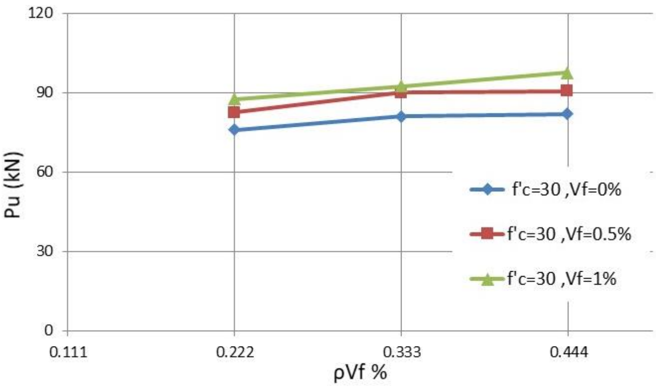

Figure 2. Effect of shear reinforcements on failure load.

Table 5. Effects of steel fibres on failure load.

Beam	V_f %	fc (MPa)	ρ_{vf} %	Failure load, Pu (kN)	Increasing Pu (%)
B30-0.5d-0	0	30	0.222	76	0
B30-0.5d-0.5	0.5			82.5	8.5
B30-0.5d-1	1			87.5	15.1
B30-0.33d-0	0	30	0.333	81	0
B30-0.33d-0.5	0.5			87.5	8
B30-0.33d-1	1			92.5	14.2
B30-0.25d-0	0	30	0.443	82	0
B30-0.25d-0.5	0.5			90.5	10.4
B30-0.25d-1	1			97.5	18.9
B50-0.5d-0	0	50	0.222	88	0
B50-0.5d-0.5	0.5			108.5	23.3
B50-0.5d-1	1			119.5	35.8
B70-0.5d-0	0	70	0.222	97	0
B70-0.5d-0.5	0.5			115.5	19.1
B70-0.5d-1	1			124.5	28.3

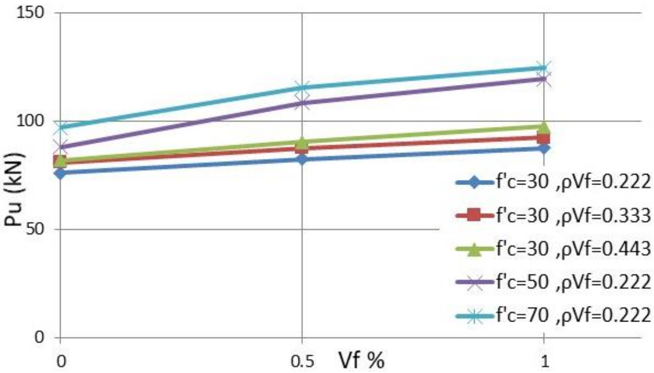

Figure 3. Effects of steel fibres on failure load.

Effect of steel fibres content

Table 5 lists the effects of steel fibres on failure load, for beams with fc' = 30 MPa and ρ_{vf} = 0.222 %, the failure load increases by 8.5 and 15.1 % in the case where the steel fibre content is raised from 0 to 0.5, and 1 %, respectively. For beams with fc' = 30 MPa and ρ_{vf} = 0.333 %, the failure load increases by 8 and 14.2 % when the steel fibre content increases from 0 to 0.5, and 1 %, respectively. For beams with fc' = 30 MPa and ρ_{vf} = 0.443 %, the failure load increases by 10.4 and 18.9 % in the case where steel fibre content increases from 0 to 0.5, and 1 %, respectively. For beams with fc' = 50 MPa and ρ_{vf} = 0.222 %, the failure load increases by 23.3 and 35.8 % in the case where the steel fibre content is raised from 0 to 0.5, and 1 %, respectively. For beams with fc' = 70 MPa and ρ_{vf} = 0.222 %, the failure load increases by 19.1 and 28.3 % when the steel fibre content is increased from 0 to 0.5, and 1 %, respectively. The larger the effect on the steel fibre is greater Fig. 3.

Effect of concrete compressive strength

Table 6 and Fig. 4 show effects of concrete compressive strength on the failure load. For beam with ρ_{vf} = 0.222 % and 0 % steel fibre content the failure load increases by 15 and 27 % in the case where the concrete strength increases from 30 to 50, and 70 MPa, respectively. For beam with ρ_{vf} = 0.222 % and 0.5 % steel fibre content the failure load increases by 31 and 40 % when the strength of the concrete increases from 30 to 50 and 70 MPa, respectively. For beam with ρ_{vf} = 0.222 and 1 % steel fibre content the failure load increases by 36 and 42 % when the concrete strength is increased from 30 to 50, and 70 MPa, respectively.

Table 6. Effect of concrete compressive strength.

Beam	V_f %	fc (MPa)	ρ_{vf} %	Failure load, Pu (kN)	Increasing Pu (%)
B30-0.5d-0	0	30	0.222	76	0
B50-0.5d-0		50		88	15
B70-0.5d-0		70		97	27
B30-0.5d-0.5	0.5	30	0.222	82.5	0
B50-0.5d-0.5		50		108.5	31
B70-0.5d-0.5		70		115.5	40
B30-0.5d-1	1	30	0.222	87.5	0
B50-0.5d-1		50		119.5	36
B70-0.5d-1		70		124.5	42

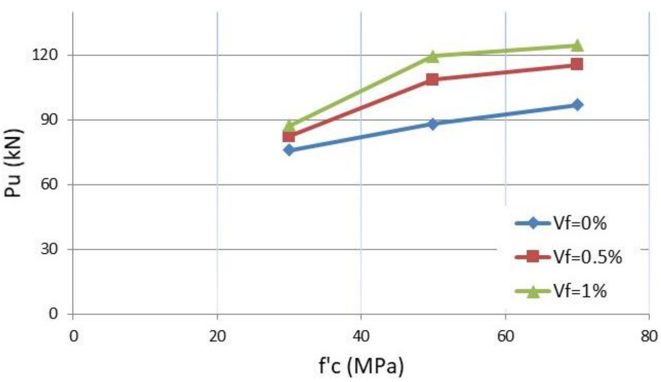

Figure 4. Effect of concrete compressive strength.

COMPARISON BETWEEN GFRP AND STEEL REINFORCEMENT

Table 7 shows the difference in experimental results of BR30-0.5d-0 and B30-0.5d-0, reinforced by the same number of stirrups and diameter, and the same concrete compressive strength at different types of reinforcements. Results show that the failure load for BR30-0.5d-0 is very close to B30-0.5d-0.

Table 7. Comparison of experimental results of beams reinforced with GFRP and steel bars.

Beam spec.	Reinf. ratio %	Reinf. type	Failure load, Pu (kN)	Ultim. defl. (mm)	Ultim. strain	Ultim. crack width (mm)
BR30-0.5d-0	0.222	steel	76.5	11.98	0.001424	1.33
B30-0.5d-0	0.222	GFRP	76	12.5	0.00193	1.56

DEFLECTION

Figures 5 to 9 show load-deflection relationships for all tested beams. It is evident that the increase in steel fibres content reduces deflection at the same load level; at 76.5 kN, the deflection decreases by 2 and 33 % for B30-0.5d-0.5 and B30-0.5d-1, respectively, as compared with B30-0.5d-0.

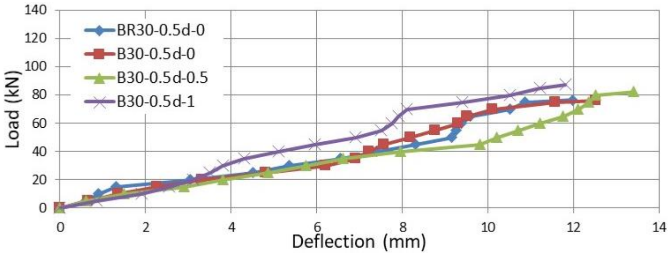

Figure 5. Load vs. experimental deflection B30-0.5d.

Also at 81 kN, deflection decreases by 15 and 17 for B30 -0.33d-0.5 and B30-0.33d-1, respectively, as compared with B30-0.33d-0.

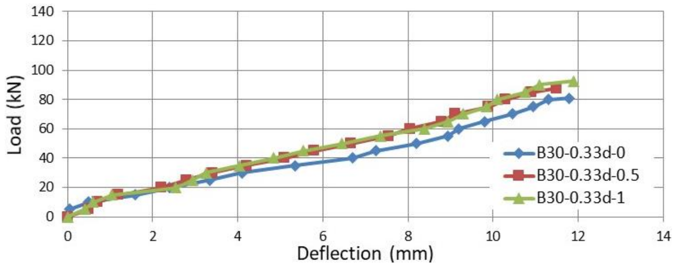

Figure 6. Load vs. experimental deflection B30-0.33d.

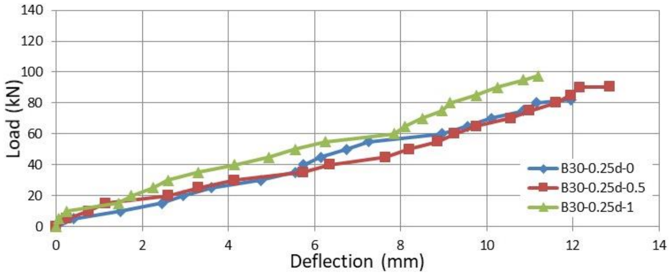

Figure 7. Load vs. experimental deflection B30-0.25d.

While at 82 kN increasing steel fibre contents from 0 to 0.5, and 1 % decreases the deflection by 3 and 31 % for B30-0.25d-0.5 and B30-0.25d-1, respectively, as compared with B30-0.25d-0.

Also at 88 kN the deflection decreases by 33 and 49 % for B50-0.5d-0.5 and B50-0.5d-1, respectively, as compared with B50-0.5d-0 due to increasing the steel fibres content from 0 to 1 %.

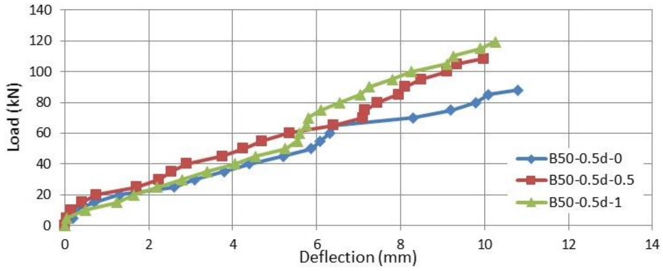

Figure 8. Load vs. experimental deflection, B50-0.5d.

On the other hand, at 97 kN, the reduction in deflection are 11 and 20 % for B70-0.5d-0.5 and B70-0.5d-1, in respect, as compared with B70-0.5d-0.

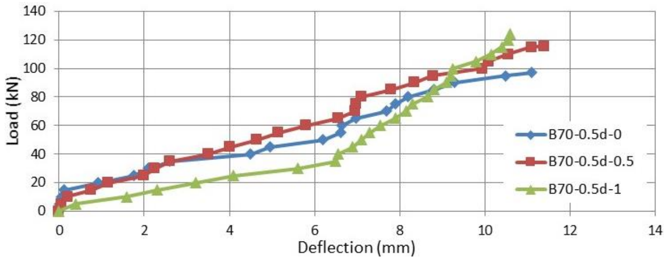

Figure 9. Load vs. experimental deflection, B70-0.5d.

CRACK WIDTH

Crack widths are measured using an analysed image by creative cloud (CC) Photoshop® software. An actual scale object reference is placed at an identical distance as is the tested beam, and after this, the image that has been captured will be analysed for predictions of crack width with a high degree of accuracy.

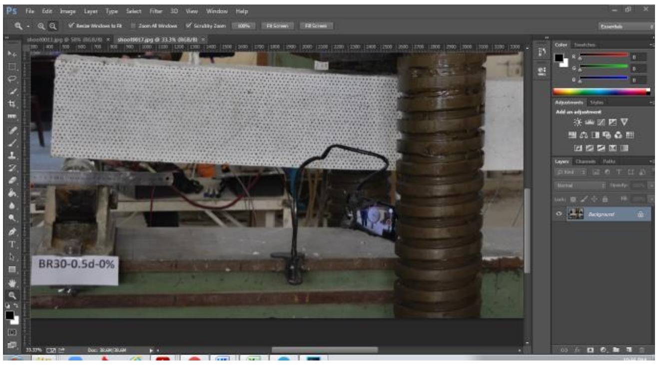

Figure 10. Crack width measurement.

Figures 11 to 15 show the load-crack relationship. The recorded results of the tests are divided into five groups based on the amount of concrete strength and shear reinforcement of the tested beam.

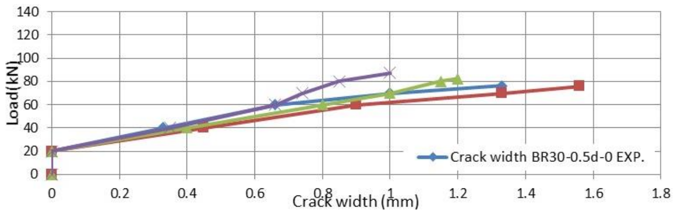

Figure 11. Load-experimental crack width of B30-0.5d.

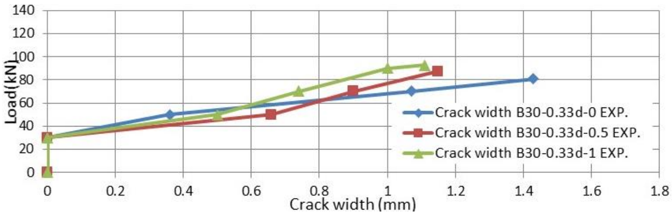

Figure 12. Load-experimental crack width of B30-0.33d.

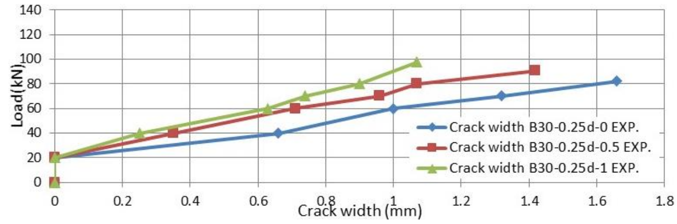

Figure 13. Load-experimental crack width of B30-0.25d.

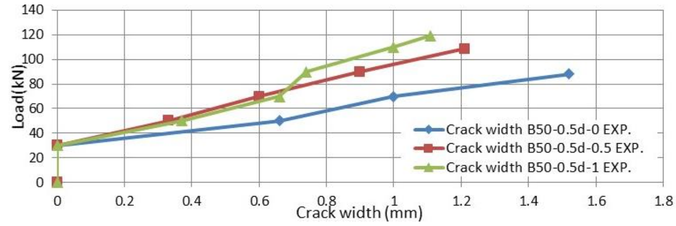

Figure 14. Load-experimental crack width of B50-0.5d.

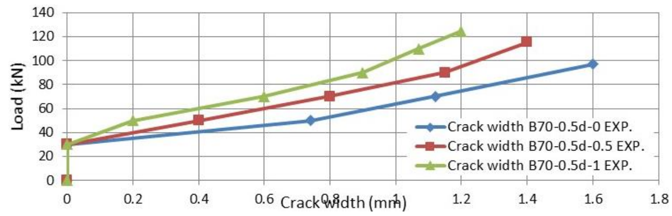

Figure 15. Load experimental crack width of B70-0.5d.

At the first crack stage, the crack load has the same value at each beam with same steel fibre content, because the width of crack at this stage depends only on concrete tensile strength. After the first crack load, the crack width would be different for each beam. This behaviour is due to the increase in the amount of stress in longitudinal reinforcement bars and increased strain in these bars.

At 76 kN, crack width decreases by 43 and 94 % for B30 -0.5d-0.5 and B30-0.5d-1, respectively, as compared with B30-0.5d-0 due to increase in steel fibre content, at 81 kN, crack width decreases by 35 and 62 % for B30-0.33d-0.5 and B30-0.33d-1, respectively, as compared with B30-0.33d-0 due to increase in steel fibre content, at 82 kN crack width decreases by 47 and 80 % for B30-0.25d-0.5 and B30-0.25d-1, in respect, as compared with B30-0.25d-0 due to the increase in steel fibre content, at 88 kN the crack width decreases by 74 and 108 % for B50-0.5d-0.5 and B50-0.5d-1, in respect, as compared with B50-0.5d-0 due to increase in steel fibre content, at 97 kN crack width decreases by 32 and 67 % for B70-0.5d-0.5 and B70-0.5d-1, respectively, as compared with B70-0.5d-0.

In addition, a comparison between experimental and theoretical crack width is investigated. The theoretical values are obtained based on ACI440-1R-06 /22/ for beams reinforced with GFRP. The calculated crack width is accorded to the equations in the mentioned codes as follows:

$$w_{cr} = 2\frac{f_f}{E_f}\beta k_b\sqrt{d_c^2 + \left(\frac{s}{2}\right)^2}, \quad \text{ACI440-1R-06}, \tag{1}$$

where: w_{cr} is crack width at beam tensile face; E_f is the elasticity modulus for reinforcement of FRP; f_f is stress in longitudinal reinforcement of FRP; β is the coefficient to the contrary size of crack that corresponds to reinforcement level to beam's tensile face; k_b is coefficient responsible for bond degree between FRP bar and surrounding concrete; ACI440.1 R-06 /22/ suggests 1.40 for deformed fibre-reinforced bars in the case where k_b is not known experimentally; d_c is concrete cover thickness measured from extreme tension fibres to a centre of closest longitudinal bars' level; and s is bar spacing. The evaluation accuracy highly relies upon the k_b value, and approximation is on the conservative side in the case where the value of $k_b = 1.40$.

The model of CEB-FIP /23/ predicts the size of the crack as follows:

$$W = \beta S_m \varepsilon_m, \tag{2}$$

where: $\beta = 1.30$; S_m is average FRP reinforced member's crack spacing; ε_m is average reinforcement strain that permits for tension stiffening as:

$$\varepsilon_m = \sigma s\left[1 - \frac{\beta_1\beta_2\left(\frac{\sigma sr}{\sigma s}\right)^2}{E_f}d\right], \tag{3}$$

where: σs is stress in the reinforcement of the tension estimated based on a cracked section; σsr is stress in the reinforcement of the tension that is evaluated according to a cracked section under load circumstances, causing the first one of the cracks; $\beta_1 = 1.0$ for high-bond bars and 0.50 for plain ones; $\beta_2 = 1$ for single short-term loading as well as 0.50 for the cyclic or sustained load.

ISIS Canada – 07 /24/ suggests the following equation for the calculation of crack width:

$$W = 2.2k_b\frac{f_f}{E_f}\frac{h_2}{h_1}\sqrt[3]{d_c A}, \tag{4}$$

where: k_b is bond-dependent coefficient, for fibre-reinforced bars with bond characteristics similar to concrete, $k_b = 1$; h_2 is distance between the outer tension surface and neutral axis (NA); h_1 is the distance between tension reinforcement centroid and NA; and A is concrete effective tension area that surrounds the reinforcement of the flexural tension and have the same centroid as this reinforcement, divided by the number of bars. Table 8 lists calculated and experimental width of the crack for all of the tested beams.

Table 8. Experimental and calculated maximal crack width.

Beam specimen	W_{exp} (mm)	W_{ACI} (mm)	$W_{CEB-FIP}$ (mm)	W_{ISIS} (mm)	W_{exp}/W_{ACI}	$W_{exp}/W_{CEB-FIP}$	W_{exp}/W_{ISIS}
B30-0.5d-0	1.56	0.75	0.34	0.98	2.08	4.6	1.6
B30-0.5d-0.5	1.23	0.73	0.52	0.95	1.68	2.37	1.3
B30-0.5d-1	1	0.54	1.58	0.71	1.9	0.63	1.41
B30-0.33d-0	1.45	1.46	1.15	1.89	0.99	1.26	0.77
B30-0.33d-0.5	1.15	1.45	1.36	1.88	0.79	0.85	0.61
B30-0.33d-1	1.09	1.39	1.53	1.81	0.78	0.71	0.6
B30-0.25d-0	1.66	1.17	0.92	1.52	1.42	1.80	1.09
B30-0.25d-0.5	1.42	1.11	1.049	1.45	1.28	1.35	0.98
B30-0.25d-1	1.07	1.20	1.59	1.56	0.89	0.67	0.69
B50-0.5d-0	1.52	1.12	1.21	1.45	1.36	1.26	1.05
B50-0.5d-0.5	1.21	1.37	1.62	1.78	0.88	0.75	0.68
B50-0.5d-1	1.15	1.04	1.71	1.35	1.11	0.67	0.85
B70-0.5d-0	1.6	0.96	0.13	1.06	1.67	12.31	1.51
B70-0.5d-0.5	1.2	1.21	1.43	1.57	0.99	0.84	0.76
B70-0.5d-1	1.11	0.92	1.53	1.20	1.21	0.73	0.93
Average					1.27	2.05	0.99

The calculated result shows that the CEB-FIP /23/ agrees with the experimental result because the CEB-FIP /23/ equation considers the strain in longitudinal bars which is affected by the parameters of the study.

Generally, all available code equations need some modifications to be applicable for high strength and fibrous concrete.

CRACK PATTERNS

The relationship between crack paths and applied load is given in Fig. 16. For beams BR30-0.5d-0, B30-0.5d-0, B30-0.5d-0.5, B30-0.5d-1, the first crack is a vertical curvature that appears at the midspan of beam (21.5, 20, 22, 23.5 kN), respectively. This crack continues to increase with applied load till it reaches the compression area. With increased load, new cracks are created on the two sides of the first crack and proceed to the compression area due to increased bending moment and shear stress. For beams B30-0.33d-0, B30-0.33d-0.5, B30-0.33d-1, the first crack is a vertical curvature that appears at midspan of the beam at 18.5, 20, 22.5 kN, respectively. This crack keeps increasing with the increase in applied load till it reaches the compression area. With an increase of load, new cracks appear on the two sides of the first crack and proceed to the compression area due to increased bending moment and shear stress. For beams B30-0.25d-0, B30-0.25d-0.5, B30-0.25d-1, the first crack is a vertical curvature that appears at midspan of the beam at 17.5, 21.5, 24 kN, respectively. This crack keeps increasing with increased applied load to the point where it reaches the compression area.

With increased load, new cracks are created on the two sides of the first crack and proceed to the compression area due to increased bending moment and shear stress. For beams B50-0.5d-0, B50-0.5d-0.5, B50-0.5d-1, the first crack is a vertical curvature that appears at midspan of the beam at 24, 25, 27 kN, respectively. This crack keeps increasing with increasing the applied load to the point where it reaches the compression area. With increased load, new cracks appear on the two sides of the first crack and proceed to the compression area due to increased bending moment and shear stress. For beams B70-0.5d-0, B70-0.5d-0.5, B70-0.5d-1, the first crack is a vertical curvature that appears at the midspan of the beam at 24, 26, 27.5 kN, respectively. This crack keeps increasing with increased applied load to the point where it reaches the compression area. With increased load, new cracks appear on the two sides of the first crack and proceed to the compression area due to increased bending moment and shear stress.

Figure 16. Crack patterns of tested beams.

FAILURE MODE

Table 3 summarizes failure modes for all of the tested beams. It is evident that increasing steel fibre content from 0 to 1 % changes the failure modes from shear to flexure-

Table 9. Comparison of experimental and calculated ultimate loads.

Beam specimens	$V_{u,exp}$ (kN)	$V_{u,ACI}$ (kN)	$V_{u,CSA}$ (kN)	$V_{u,ISIS}$ (kN)	$V_{u,Tureyen}$ (kN)	$V_{u,exp}$/$V_{u,ACI}$	$V_{u,exp}$/$V_{u,CSA}$	$V_{u,exp}$/$V_{u,ISIS}$	$V_{u,exp}$/$V_{u,Tureyen}$
BR30-0.5d-0	38.25	38.67	24.3	28.58	34.65	0.99	1.57	1.34	1.10
B30-0.5d-0	38	38.67	24.3	28.58	34.65	0.98	1.56	1.33	1.1
B30-0.5d-0.5	41.25	40.05	25.29	29.63	37.285	1.03	1.63	1.4	1.11
B30-0.5d-1	43.75	41.07	26	30.42	39.275	1.07	1.68	1.43	1.11
B30-0.33d-0	40.5	49.08	26.54	36	34.65	0.83	1.53	1.13	1.17
B30-0.33d-0.5	43.75	50.45	27.53	37.05	37.285	0.87	1.59	1.18	1.17
B30-0.33d-1	46.25	51.47	28.3	37.84	39.275	0.9	1.63	1.22	1.18
B30-0.25d-0	40.25	59.5	28.79	43.43	34.65	0.67	1.4	0.93	1.16
B30-0.25d-0.5	45.25	60.85	29.78	44.48	37.285	0.74	1.52	1.02	1.21
B30-0.25d-1	48.75	61.87	30.52	45.27	39.275	0.79	1.59	1.08	1.24
B50-0.5d-0	44	43.49	27.71	32.28	43.95	1.01	1.59	1.36	1
B50-0.5d-0.5	54.25	45.2	28.86	33.58	47.27	1.2	1.88	1.62	1.15
B50-0.5d-1	59.75	46.57	29.76	34.64	49.925	1.3	2	1.72	1.2
B70-0.5d-0	48.5	47.73	30.52	35.53	52.185	1.02	1.59	1.37	0.93
B70-0.5d-0.5	57.75	48.84	31.22	36.38	54.335	1.18	1.85	1.59	1.06
B70-0.5d-1	62.25	49.82	32.84	37.13	56.215	1.25	1.89	1.68	1.11
average						0.99	1.66	1.34	1.12

shear failure, which is more safe and ductile. Also, by increasing the shear reinforcement ratio from 0.222 to 0.443 % converts the failure modes from shear to flexure-shear failure regardless of steel fibre content. However, the results show that the compressive strength of the concrete does not affect failure modes; also, the use of GFRP stirrups has no impact on failure modes compared with reference beams.

THEORETICAL PREDICTION OF ULTIMATE LOAD

In the present study, the theoretical ultimate load Vu of GFRP reinforced beams is calculated according to shear design formulas included in the Appendix to verify the validity of these formulas.

Table 9 lists experimental and calculated results of the ultimate load. The calculation equations are given by ACI4 40.1R-15 /25/, CSA S 806-12 /26/, ISIS /24/, and Tureyen /27/ show good agreement of beam flexural strength.

CSA S806-12 /26/ and ISIS-07 /24/ codes show conservative results, while ACI440-1R-15 /25/ and Tureyen /27/ equation shows good agreement in the outcome when compared with experimental results.

CONCLUSIONS

By increasing shear reinforcement ratio from 0.222 to 0.333 % increases the failure load by 2, 6 and 5 % for steel fibre content 0, 0.5, and 1 %, respectively, while increasing shear reinforcement ratio from 0.222 to 0.443 % increases the failure load by 8, 10, and 11 % for steel fibre content 0, 0.5, and 1 %, respectively.

Increasing the compressive strength of the concrete from 30 to 50 MPa increases the failure load by 14, 32, and 37 % for steel fibre content 0, 0.5, and 1 %, respectively, while increasing the compressive strength of the concrete from 30 to 70 MPa increases the failure load by 28, 40, and 42 % for steel fibre content 0, 0.5, and 1 %, respectively.

Increasing steel fibre content 0 to 0.5, and 1 % increases the failure load by 8.5 and 15.1 %, 8 and 14.2 %, and 10.4 and 18.9 %, for beams with ρ_{vf} = 0.222, 0.333 and 0.443 %, respectively.

The use of GFRP stirrups has a very marginal effect on the failure load. Increasing steel fibres contents from 0 to 1 % changes the mode of failure from shear to flexure-shear failure, which has been found more safe and ductile. Also, increasing the shear reinforcement ratio from 0.222 to 0.443 % converts failure mode from shear to flexure-shear failure, regardless of steel fibres content.

The increase in steel fibres content loads decreases the strain in longitudinal GFRP bars, between 4-56 %.

The increases in concrete compressive strength from 30 to 70 MPa decreases the strain in longitudinal GFRP bars between 40-74 %.

The increase in steel fibres content leads to a decrease in the strain in GFRP stirrups between 14-140 %.

Increase in compressive strength value of concrete from 30 to 70 MPa decreases the strain in GFRP stirrups between 60-125 %.

The increase in shear reinforcement ratio from 0.222 to 0.443 % decreases the strain in stirrups GFRP bars between 5-64 %.

Crack width decreases by 35-94 % when the steel fibre content increases from 0 to 1 % for beam with $f'c$ = 30 MPa.

Crack width decreases by 74-108 % when steel fibre content increases from 0 to 1 % for beam with $f'c$ = 50 MPa.

Crack width decreases by 32-67 % when steel fibre content increases from 0 to 1 % for beam with $f'c$ = 70 MPa.

The calculated result showed that the CEB-FIP agrees with the experimental result because the CEB-FIP equation considers the strain in longitudinal bars, which is affected by the study's parameters.

The experimental and calculated ultimate shear load comparison showed that the CSA and ISIS codes results were very conservative, with safety factor reaching 66%. In contrast, the ACI and Tureyen equation code results showed good agreement with the experimental results.

APPENDIX

Prediction methods	Equations for shear strength
ACI 440.1R-15/25/	$V_c = \frac{2}{5}\sqrt{f_c'} b_w k d$, where: V_c is shear resistance provided by concrete; b_w is width of web (mm); f_c' is concrete compressive strength (MPa); d is effective depth (mm); $c = kd$, cracked transformed section neutral axis depth (mm) $k = \sqrt{2\rho n + \rho n^2} - \rho n$, $\rho = \frac{A}{b_w d}$, A is area of tensile reinforcement (mm^2) $V_f = \frac{A_{fv} f_{fv} d}{s}$, where: V_f is shear resistance provided by FRP stirrups; A_{fv} is area of shear reinforcement within stirrups spacing s (mm^2); ffv is tensile strength of FRP taken as the smallest of design tensile strength f_{fu}; f_{fb} is strength of bent portion of FRP stirrups, or stress corresponding to $0.004E_f$ (MPa); s - spacings of FRP stirrups.
CSA -S806-12/26/	$V_c = 0.05\lambda k_m k_r (f_c')^{1/3} b_w d_v$ for $d \le 300$ mm provided that $0.11\sqrt{f_c'} b_w d_v \le V_c \le 0.22\sqrt{f_c'} b_w d_v$ $k_m = \sqrt{\frac{V_f d}{M_f}} \le 1.0$, where $\frac{V_f d}{M_f}$ is equivalent to $\frac{d}{a}$; $k_r = 1 + (E_f \rho)^{1/3}$; E_f is elastic modulus of the longitudinal FRP reinforcement; d_v is taken as the larger of $0.9d$ or $0.72h$; h is overall thickness of a member; V_f is ultimate shear; M_f is ultimate moment

	$V_f = \frac{0.4\phi_f A_{fv} f_{fu} dv}{s}\cot\theta$; $f_{fu} \le 0.005E_f$; $\theta = 30° + 7000\varepsilon_l$ provided that $30° \le \theta \le 60°$; $\varepsilon_l = \frac{M_f dv + V_f + 0.5N_f}{E_f A_{fv}}$; N_f is axial load normal to the member cross section, in our case = 0.
JSCE -97 /12/	$V_c = \beta_d \beta_p \beta_n f_{vcd} b_w d / \gamma_b$, where: $\beta_n = \left(\frac{1000}{d}\right)^{1/4} \le 1.5$; $\beta_p = \left(\frac{1000\rho E}{E_s}\right)^{1/4} \le 1.5$; E_s is elastic modulus for steel (200 kN/mm^2), $\beta_n = 1$ if no axial force applied; $f_{vcd} = 0.2\sqrt[3]{f_c'}$ provided that $f_{vcd} \le 0.72$ N/mm^2; $\gamma_b = 1.3$; $V_f = [A_{fv}E_{fv}\varepsilon_{fwd}(\cos\alpha_s + \sin\alpha_s)/s]z/\gamma_b$; E_{fv} is elastic modulus of the FRP shear reinforcement; α_s is angle formed by shear reinforcement and member axis; $z = d/1.15$; $\gamma_{bs} = 1.15$; $\varepsilon_{fwd} = 0.0001\left(f'_{mcd}\frac{\rho E_f}{\rho_w E_{fv}}\right)^{1/2}\left[1 + 2\left(\frac{\sigma_n}{f'_{mcd}}\right)\right]$; $\rho_w = \frac{A_{fv}}{b_w s}$; $f'_{mcd} = \left(\frac{h}{0.3}\right)^{1/10} f'c$
ISIS -07 /24/	$V_c = 0.2\lambda\sqrt{f_c'}b_w d\sqrt{\frac{E_f}{E_s}}$, $V_f = \frac{A_{fv} f_{fv} dv\cot\theta}{s}$, $d_v = 0.9d$, $ffv = \frac{\left(0.05\frac{rb}{db} + 0.3\right)f_{fuv}}{1.5}$ or $ffv = E_{fv}\varepsilon_{fwd1}$, $\varepsilon_{fwd} = 0.0001\left(f'_{mcd}\frac{\rho E_f}{\rho_w E_{fv}}\right)^{1/2}\left[1 + 2\left(\frac{\sigma_n}{f'_{mcd}}\right)\right]$
Nehdi et al. /28/	Optimized equation: If $\frac{a}{d} \ge 2.5$: $V_c = 2.1\left(\frac{f_c'\rho_{fl} d}{a}\frac{E_{fl}}{E_s}\right)^{0.23} bd$ If $\frac{a}{d} < 2.5$: $V_c = 2.1\left(\frac{f_c'\rho_{fl} d}{a}\frac{E_{fl}}{E_s}\right)^{0.23} bd \cdot \frac{2.5d}{a}$; $\rho_{fl} = \frac{A_{fl}}{bd}$; $V_{fv} = 0.74(\rho_{fv} f_{fv})^{0.51} bd$; $\rho_{fv} = \frac{A_{fv}}{bs}$ Optimized equation: If $\frac{a}{d} \ge 2.5$: $V_c = 2.1\left(\frac{f_c'\rho_{fl} d}{a}\frac{E_{fl}}{E_s}\right)^{0.3} bd$ If $\frac{a}{d} < 2.5$: $V_c = 2.1\left(\frac{f_c'\rho_{fl} d}{a}\frac{E_{fl}}{E_s}\right)^{0.3} bd \cdot \frac{2.5d}{a}$; $\rho_{fl} = \frac{A_{fl}}{bd}$; $V_{fv} = 0.5(\rho_{fv} f_{fv})^{0.5} bd$; $\rho_{fv} = \frac{A_{fv}}{bs}$
Hoult et al. /29/	$V_c = \beta\sqrt{f_c'}bd_v$, where: $\beta = \frac{0.30}{0.5 + (1000\varepsilon_x + 0.15)^{0.7}} \cdot \frac{1300}{1000 + s_{ze}}$; $d_v = 0.9d$; $s_{xe} = \frac{31.5d}{16 + a_g} \ge 0.77d$; $a_g = \begin{cases} a_g, & \text{if } f_c' < 60 \\ a_g - \frac{a_g}{10}(f_c' - 60), & \text{if } 60 \le f_c' < 70 \\ 0, & \text{if } f_c' > 70 \end{cases}$; $\varepsilon_x = \frac{\left(\frac{M_f}{d_v}\right) + V_f}{2(E_s A_s)}$
Tureyen and Frosch /27/	Calculations are in English units. $V_c = \left(\sqrt{16 + \frac{4\sigma_m}{3\sqrt{f_c'}}}\right)\sqrt{f_c'}bc$, where: $c = kd$; $\sigma_m = \frac{f_{cr} Ikd}{I_{cr}\left(\frac{h}{2}\right)}$; $I_{cr} = b\left(\frac{kd}{3}\right)^3 + n_f A_f (d - kd)^2$; $I = \frac{h^3 b}{12}$; $f_{cr} = 0.6\lambda\sqrt{f_c'}$; $k = \sqrt{2\rho_{fl} n_f + (\rho_{fl} n_f)^2} - \rho_{fl} n_f$

REFERENCE

1. Bentz, E.C., Massam, L., Collins, M.P. (2010), *Shear strength of large concrete members with FRP reinforcement*, J Compos. Constr. 14(6): 637-646. doi: 10.1061/(ASCE)CC.1943-5614.0000108
2. Imjai, T., Guadagnini, M., Garcia R., Pilakoutas, K. (2016), *A practical method for determining shear crack induced deformation in FRP RC beams*, Eng. Struct. 126: 353-364. doi: 10.1016/j.engstruct.2016.08.007
3. Mahmoud, K., El-Salakawy, E. (2015), *Shear strength of glass fiber reinforced polymer-reinforced concrete continuous beams without transverse reinforcement*, Can. J Civ. Eng. 42(12): 1073-1082. doi: 10.1139/cjce-2014-0238
4. Razaqpur, A.G., Shedid, M., Isgor, B. (2011), *Shear strength of fiber-reinforced polymer reinforced concrete beams subject to unsymmetric loading*, J Compos. Constr. 15(4): 500-512. doi: 10.1061/(ASCE)CC.1943-5614.0000184
5. Shehata, E., Morphy, R., Rizkalla, S. (2000), *Fiber reinforced polymer shear reinforcement for concrete members: behaviour and design guidelines*, Can. J Civ. Eng. 27(5): 859-872. doi: 10.1139/l00-004
6. Nagasaka, T., Fukuyama, H., Tanigaki, M. (1995), *Shear performance of concrete beams reinforced with FRP stirrups*, In: Proc. Int. Symp. on Fibre Reinforced Plastic Reinforcement for Concrete Structures, Vol.138: 789-811.
7. Ahmed, E.A., El-Sayed, A.K., El-Salakawy, E., Benmokrane, B. (2010), *Bend strength of FRP stirrups: comparison and evaluation of testing methods*, J Compos. Constr. 14(1): 3-10. doi: 10.1061/(ASCE)CC.1943-5614.0000050
8. Shehata, E.F.G., *Fiber-reinforced polymer (FRP) for shear reinforcement in concrete structures*, Ph.D. Thesis, University of Manitoba, Winnipeg, Manitoba, Canada, 1999.
9. ACI Committee 222, Protection of Metals in Concrete Against Corrosion (ACI 222R-01), ACI Manual of Concrete Practice, American Concrete Institute, Farmington Hills, MI.
10. Zoghi, M. (Ed.), The International Handbook of FRP Composites in Civil Engineering, 1st Ed., CRC Press, Boca Raton, 2013. doi: 10.1201/b15806
11. Balaguru, P., Nanni, A., Giancaspro, J., FRP Composites for Reinforced and Prestressed Concrete Structures, 1st Ed., Taylor & Francis Group, CRC Press, London, 2009. doi: 10.1201/9781482288537
12. Machida, A. (Ed.), Recommendation for Design and Construction of Concrete Structures Using Continuous Fiber Reinforcing Materials, Japan Society of Civil Engineers, Concrete Eng. Ser. vol.23; Tokyo, Japan Society of Civil Engineers, 1997.
13. Joint ASCE-ACI Task Committee 426 (1973), *The shear strength of reinforced concrete members*, J Struct. Div. 99(6): 1091-1188. doi: 10.1061/JSDEAG.0003532
14. Mousa, S., Mohamed, H.M., Benmokrane, B. (2019), *Strength and deformability aspects of circular concrete members reinforced with hybrid carbon-FRP and glass-FRP under flexure*, J Compos. Constr. 23(2): 04019005. doi: 10.1061/(ASCE)CC.1943-5614.0000931
15. El-Nemr, A., Ahmed, E.A., El-Safty, A., Benmokrane, B. (2018), *Evaluation of the flexural strength and serviceability of concrete beams reinforced with different types of GFRP bars*, Eng. Struct. 173: 606-619. doi: 10.1016/j.engstruct.2018.06.089
16. Ahmed, E.A., Settecasi, F., Benmokrane, B. (2014), *Construction and testing of GFRP steel hybrid-reinforced concrete bridge-deck slabs of Sainte-Catherine overpass bridges*, J Bridge Eng. 19(6): 04014011. doi: 10.1061/(ASCE)BE.1943-5592.0000581
17. Abdullah, M.M., Hassan, H.F. (2021), *Flexural behavior of normal and high strength continuous beams reinforced by GFRP bars*, J Eng. Sustain. Develop. 25(1): 15-30. doi: 10.31272/jeasd.25.1.2
18. Kotynia, R., Kaszubska, M., Barros, J.A.O. (2018), *Shear behavior of steel or GFRP reinforced concrete beams without stirrups*, In: Hordijk D., Luković M. (Eds.), High Tech Concrete: Where Technology and Engineering Meet, Springer, Cham, 2018: 769-777. doi: 10.1007/978-3-319-59471-2_90
19. Jumaa, G.B., Yousif, A.R. (2019), *Size effect on the shear failure of high-strength concrete beams reinforced with basalt FRP bars and stirrups*, Constr. Build. Mater. 209: 77-94. doi: 10.1016/j.conbuildmat.2019.03.076
20. Li, W., Tang, S., Huang, Z., et al. (2020), *Shear behavior of concrete beam reinforced in shear with carbon fiber-reinforced polymer mesh fabric (CFRP-MF) configuration*, Eng. Struct. 218: 110828. doi: 10.1016/j.engstruct.2020.110828
21. ACI 211.1-91 (1991), Standard practice for selecting proportions for normal, heavyweight, and mass concrete, ACI Committee 211, Farmington Hills, MI, USA.
22. ACI 440.1 R-06. Guide for the Design and Construction of Structural Concrete Reinforced with FRP Bars, American Concrete Institute, 2006.
23. CEB-FIP, FRP reinforcement in RC structures, Fib bulletin 40, Tech. Report, Int. Federation for Structural Concrete (fib), 2007.
24. ISIS Canada Research Network, Reinforcing Concrete Structures with Fiber Reinforced Polymers, Design Manual No.3 Ver.2, Canada ISIS Canada Corporation, Manitoba, 2007.
25. ACI 440.1R-15, Guide for the Design and Construction of Structural Concrete Reinforced with FRP Bars, American Concrete Institute, Farmington Hills, MI, USA, 2015.
26. CSA, S806-12 (R2017): Design and construction of building structures with fibre-reinforced polymers, Canadian Standards Association Group, Canada, 2012, Reaffirmed in 2017.
27. Yost, J.R., Gross, S.P., Dinehart, D.W. (2001), *Shear strength of normal strength concrete beams reinforced with deformed GFRP bars*, J Compos. Constr. 5(4): 268. doi: 10.1061/(ASCE)1090-0268(2001)5:4(268)
28. Nehdi, M., El Chabib, H., Aly Saïd, A. (2007), *Proposed shear design equations for FRP-reinforced concrete beams based on genetic algorithms approach*, J Mater. Civ. Eng. 19(12): 1033-1042. doi: 10.1061/(ASCE)0899-1561(2007)19:12(1033)
29. Hoult, N.A., Sherwood, E.G., Bentz, E.C., Collins, M.P. (2008), *Does the use of FRP reinforcement change the one-way shear behavior of reinforced concrete slabs?*, J Compos. Constr. 12(2): 125-133. doi: 10.1061/(ASCE)1090-0268(2008)12:2(125)